Spectroscopy near the proton drip line in the deformed $A=130$ mass region: The ^{126}Pr nucleus

C. M. Petrache,[1] M. Nespolo,[2] S. Brant,[3] G. Lo Bianco,[1] D. Bazzacco,[2] S. Lunardi,[2] P. Spolaore,[4] M. Axiotis,[4] N. Blasi,[5] G. de Angelis,[4] T. Kröll,[2] N. Marginean,[4] T. Martinez,[4] R. Menegazzo,[2] D. R. Napoli,[4] B. Quintana,[2] A. Saltarelli,[1] A. Ventura,[6] and D. Vretenar[3]

[1]*Dipartimento di Matematica e Fisica, University of Camerino, Camerino, Italy*
[2]*Dipartimento di Fisica and INFN, Sezione di Padova, Padova, Italy*
[3]*Department of Physics, Faculty of Science, University of Zagreb, Zagreb, Croatia*
[4]*INFN, Laboratori Nazionali di Legnaro, Legnaro, Italy*
[5]*INFN, Sezione di Milano, Milano, Italy*
[6]*Centro Dati Nucleari, ENEA, Bologna, Italy*

(Received 21 May 2001; published 19 September 2001)

The near proton drip-line nucleus ^{126}Pr was studied via in-beam γ-ray spectroscopy using the ^{40}Ca $+^{92}$Mo reaction at 190 MeV. We observed for the first time excited states above the known isomer in this nucleus, up to spin $31\hbar$. The observed band is assigned to a $\pi h_{11/2}\otimes\nu h_{11/2}$ configuration and is discussed in the framework of the interacting boson-fermion-fermion model. The calculations and the experimental information suggest a spin 8^+ for the lowest observed state. With such a spin assignment the moment of inertia of ^{126}Pr gets larger than in the heavier Pr isotopes, suggesting a sudden change in deformation close to the proton drip line.

DOI: 10.1103/PhysRevC.64.044303 PACS number(s): 21.10.Re, 21.60.Cs, 27.60.+j

I. INTRODUCTION

Very recently, the proton radioactivity from ^{131}Eu and ^{141}Ho has been identified [1] and the decay rate deviates significantly from calculations assuming spherical configurations, thus indicating the onset of large deformations in the drip line nuclei below $Z=69$. Predictions by the microscopic-macroscopic mass model [2] and by relativistic mean field calculations [3] support these experimental results and suggest the position of the proton drip line. The lifetimes of the proton-decaying isomers are extremely sensitive to the orbital angular momentum l of the emitted proton and can vary over several orders of magnitude when changing the angular momentum of the occupied orbital. The position of certain orbitals at the Fermi surface depends strongly on the β_2 deformation [4]. It is therefore very important to determine the quadrupole deformation of the nuclei at and beyond the proton drip line, in order to locate the orbitals close to the Fermi surface and to estimate the lifetime of the isomers, which is essential when looking for new proton emitters. The deformation of the nuclei at the proton drip line in the $A=130$ mass region can be experimentally tested by comparing the lifetimes of proton emitters with theoretical predictions and by investigating the level structure of particle bound nuclei close to the drip line. For $Z=59$ the proton drip line is predicted to correspond to the isotopes ^{124}Pr [3], while the lighter, ^{123}Pr nucleus lies on the line defined by the known proton emitters in a N-Z map [5]. The lightest Pr nucleus for which spectroscopic information has been published is ^{127}Pr [6], while the lightest odd-odd Pr nucleus with known excited states is ^{128}Pr [7].

In order to investigate the variation of the deformation when approaching the proton drip-line, we have studied the ^{126}Pr nucleus in an experiment performed with the GASP array [8]. The level structure of ^{126}Pr was not known before our experiment. The only information reported previously came from three β-decay studies by Nitschke *et al.* [9], Barnéoud *et al.* [10], and Osa *et al.* [11]. From these β-decay studies it was concluded that the isomer which decays by β^+/EC to excited states in ^{126}Ce has a half-life of 3.14(22) sec [11] and spin $I\geqslant(5,6)$ [10].

We have observed for the first time, in the experiment presented in this paper, excited states in the ^{126}Pr nucleus; they are members of a strongly coupled band with a probable $\pi h_{11/2}\otimes\nu h_{11/2}$ configuration. We also observed a double decoupled band belonging to either ^{125}Pr or ^{126}Pr. These results, including the level schemes, have been already presented at various conferences [12,13]. Very recently, a paper presenting the same rotational bands observed in our experiment and assigned to ^{126}Pr has appeared [14], in which also the $\pi h_{11/2}\otimes\nu h_{11/2}$ band of ^{128}Pr is discussed. We like to mention here that, due to the superior performances of our setup in the low-energy range, we observed low energy transitions at the bottom of all three bands reported in Ref. [14]. In the present paper we will discuss only the $\pi h_{11/2}\otimes\nu h_{11/2}$ band firmly assigned to ^{126}Pr. The observed doubly decoupled band, tentatively assigned to ^{126}Pr in Ref. [14] was too weakly populated and could not be firmly assigned to a specific Pr nucleus.

II. EXPERIMENTAL DETAILS

We populated high-spin states in ^{126}Pr using the ^{40}Ca $+^{92}$Mo reaction, with a ^{40}Ca beam of 5 pnA intensity and an energy of 190 MeV. The beam was provided by the XTU Tandem accelerator of the Laboratori Nazionali di Legnaro. The target was a self-supporting ^{92}Mo foil with a thickness of 0.5 mg/cm^2. The experimental setup consisted of the GASP array for γ-ray detection, the ISIS ball for charged particle detection [15] and the recoil mass spectrometer (RMS) CAMEL for mass identification [16]. The GASP ar-

ray with 40 Compton-suppressed Ge detectors and the 80-element BGO ball was used for a γ^n coincidence measurement. The experimental arrangement in GASP has been carefully prepared, in order to minimize the absorbtion of the low-energy x rays. Improvements in the Ge detector performances by replacing the standard preamplifiers with new ones, and the tuning of the signal processing electronics to maximize the detector efficiency in the energy range below 50 keV increased the coincidence rate between the x and γ rays. Light charged particles (p, d, t, and α particles) were detected with the ISIS ball, which is composed of 40 $\Delta E - E$ Si telescopes. The recoiling nuclei leaving the target foil were focused through the r.m.s. to the parallel plate avalanche counter (PPAC) mounted at the focal plane, which provided the mass identification (via A/q) of the spatially separated recoil nuclei. Events were written on tape when two or more Ge detectors fired in coincidence with at least two BGO detectors. A total of 3.5×10^9 Compton-suppressed events have been collected, out of which 26.2×10^6 were in coincidence with the PPAC signals.

The ^{126}Pr nucleus was populated via the αpn channel. The charged particles from each event were identified mainly as protons and α particles and their energy measured. The events were then sorted according to the number of charged particle detectors that fired in coincidence. For each charged-particle combination, i.e., $1p, 2p, 3p, 4p, \alpha p, \alpha 2p, 2\alpha, 2\alpha p$, E_γ-E_γ, and E_γ-E_γ-E_γ matrices were produced off-line for further analysis. The level structure of ^{126}Pr has been derived from the analysis of the αp-gated data.

III. RESULTS

The results of our in-beam measurements give the first experimental evidence of excited states above the known isomer in ^{126}Pr [12,13]. The coincidence spectrum of a new band assigned to ^{126}Pr is given in Fig. 1. It was obtained from the αp-matrix by summing the gates on two clean γ-rays (105 and 143 keV). The assignment of the observed γ-ray cascade to the ^{126}Pr residual nucleus was done using the following procedure. The use of RMS enabled the selection of the recoiling evaporation residues as a function of their mass-to-charge ratio (A/q). The charge-state ambiguity which remained due to similar A/q ratios for A and $A-4$ nuclei with charge-state q and $q-1$ [e.g., $A/q=130/30 \approx (A-4)/(q-1)=126/29\approx4$] have been removed by means of the coincidence with charged particles detected in the ISIS ball. The isotopes with different nuclear charge Z contributing to a given A/q detected at the focal plane of r.m.s. have been distinguished by means of the coincidence x rays as measured by the GASP detectors. The selection with respect to the number and type of evaporated charged particles performed with ISIS was also used to improve the γ-ray resolution by a kinematic correction (through the reconstruction of the recoil direction using the detection of charged particles in ISIS).

When applying the above procedure to the case of ^{126}Pr, we first observe that the clean spectrum shown in Fig. 1 contains the K_α and K_β x rays of the Pr isotope. An expansion of the low-energy part of the spectrum is given in Fig. 2,

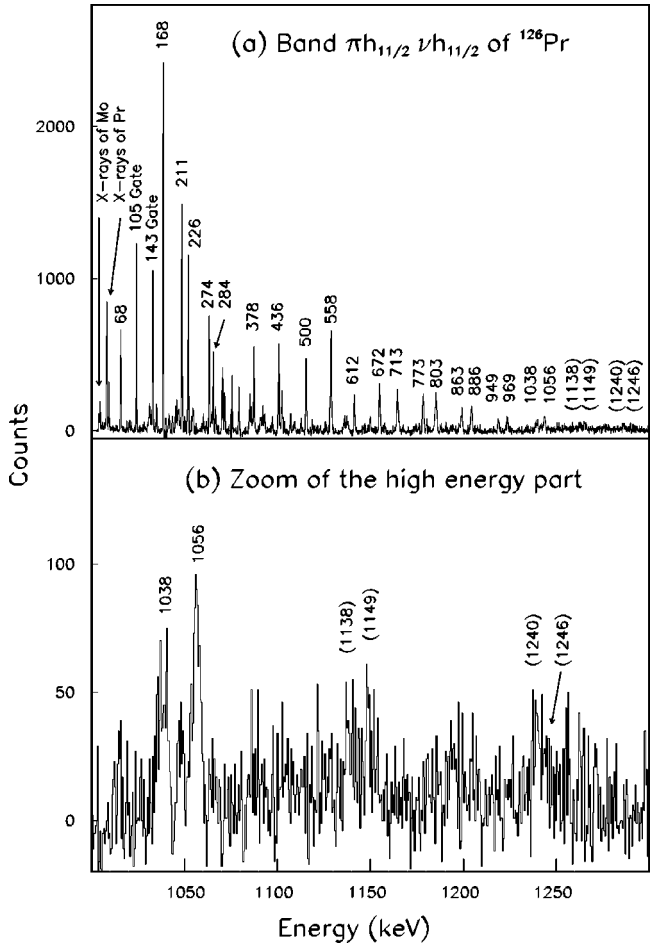

FIG. 1. Coincidence $\gamma\gamma$ spectrum obtained from the αp matrix by summing the gates on the 105 and 143 keV transitions.

where properly normalized spectra of ^{125}La and ^{126}Ce are superposed for comparison. As one can see, the optimum resolution of the GASP array in the low-energy region enabled the separation of peaks differing by about 1 keV, al-

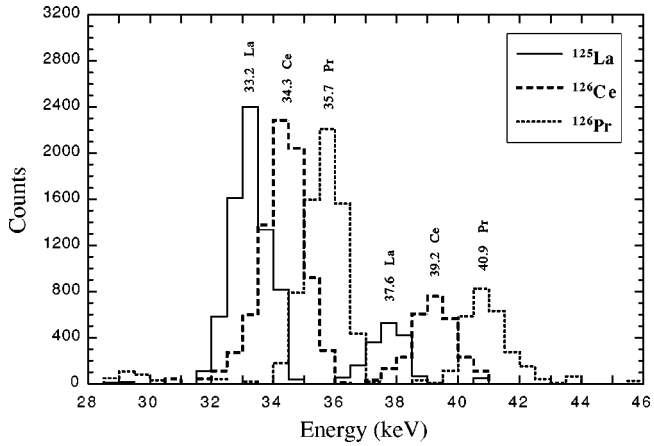

FIG. 2. A superposition of the low-energy part of the spectra in coincidence with clean γ rays of ^{125}La, ^{126}Ce, and ^{126}Pr, which shows the good separation of the x rays belonging to different isotopes.

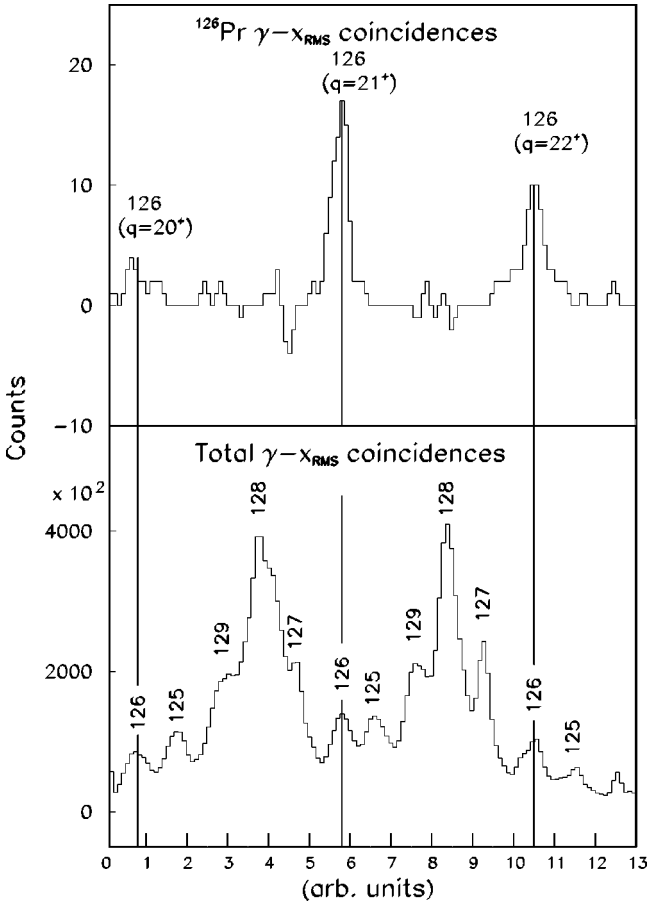

FIG. 3. Spectra from the PPAC detector mounted at the focal plane of the recoil mass spectrometer, projected on the horizontal direction. The upper spectrum is in coincidence with clean γ rays assigned to ^{126}Pr, while the lower one is in coincidence with all γ rays detected by GASP. The peaks are marked with the mass number and the charge state of the recoiling nuclei.

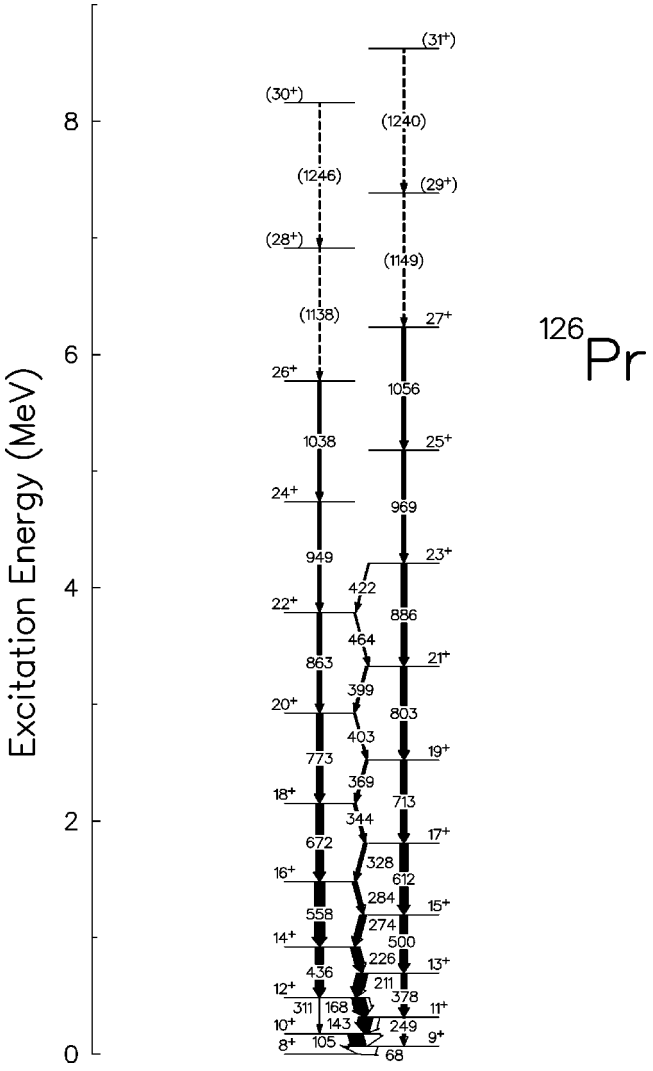

FIG. 4. Level scheme of ^{126}Pr deduced from the present work. The transition intensities are proportional to the width of the arrows.

lowing us to assign the observed cascade to a Pr isotope. Another indication that the observed band belongs to a Pr nucleus, was obtained by comparing spectra generated by gating on the same 105 and 143 keV transitions on matrices in coincidence with different combinations of charged particles detected in the ISIS ball: the spectrum obtained from the αp matrix was not present in the matrices in coincidence with more than one α particle and/or one proton, indicating the parentage with a Pr nucleus. The mass number of the Pr nucleus to which the observed band belongs was determined using the mass separation produced at the focal plane of r.m.s. As one can see in Fig. 3, from the high yield of the PPAC in coincidence with γ rays detected in GASP (projection on the x axis), only a few counts remains when gating on the clean 105 and 143 keV γ rays of the observed band. Almost all counts are concentrated at the three charge-state positions where the $A=126$ recoils are focused, indicating that the Pr recoils have mass 126.

The decay scheme of ^{126}Pr resulting from the present analysis is shown in Fig. 4. Information about the transition intensities and the DCO ratios are given in Table I. The spins of the new levels have been inferred (when possible) from a directional correlation orientation (DCO) analysis as described, e.g., in Ref. [17].

For the low-energy transitions of 68, 105, and 143 keV, information on their electric or magnetic character, as well as the multipole order, could be derived from intensity balance consideration. By gating from above (for example, the 168 keV transition) the total intensity of two consecutive transitions (143 and 105 keV) must be the same. By correcting the gamma intensity, observed in this gated spectrum, with the corresponding conversion coefficent for electric or magnetic character and for multipole order up to three, only the combination $M1$-$M1$ gives the same total intensity for both transitions. This analysis has been done by gating on the 168 and 143 keV transitions, allowing us to assign firm $M1$ character to the three low-energy transitions of the level scheme of Fig. 4.

For the spin assignment, the assumption has been made that the band-head has spin parity 8^+. The arguments for this assignment are given in the discussion below.

TABLE I. γ-ray energies, intensities, DCO ratios, and assignment for transitions in ^{126}Pr.

E_γ (keV)	Transition intensities[a]	DCO ratios	Assignment[b] $I_i^\pi \rightarrow I_f^\pi$
68.2	20(2)	1.1(4)[c]	$9^+ \rightarrow 8^+$
105.4	42(4)	1.06(28)[c]	$10^+ \rightarrow 9^+$
143.2	40(2)	0.51(11)[d]	$11^+ \rightarrow 10^+$
167.7	38(2)	0.62(3)[d]	$12^+ \rightarrow 11^+$
210.9	27.5(9)	0.63(35)[d]	$13^+ \rightarrow 12^+$
225.7	23(0.8)	0.52(4)[d]	$14^+ \rightarrow 13^+$
248.6	8(4)		$11^+ \rightarrow 9^+$
274.1	17.6(7)	0.57(12)[d]	$15^+ \rightarrow 14^+$
284.1	12.1(6)	1.08(61)[c]	$16^+ \rightarrow 15^+$
310.9	15(3)		$12^+ \rightarrow 10^+$
328.1	9.5(5)		$17^+ \rightarrow 16^+$
343.8	7.9(4)		$18^+ \rightarrow 17^+$
369.4	7.2(8)		$19^+ \rightarrow 18^+$
378.4	17(1)		$13^+ \rightarrow 11^+$
399.1	6.5(4)		$21^+ \rightarrow 20^+$
403.4	4.8(4)		$20^+ \rightarrow 19^+$
421.7	3.8(4)		$23^+ \rightarrow 22^+$
436.3	22(0.9)		$14^+ \rightarrow 12^+$
464.0	4.2(4)		$22^+ \rightarrow 21^+$
499.9	21(0.8)	1.06(35)[d]	$15^+ \rightarrow 13^+$
558.3	29(0.9)		$16^+ \rightarrow 14^+$
612.4	22(5)		$17^+ \rightarrow 15^+$
671.7	21(2)		$18^+ \rightarrow 16^+$
713.4	19(1)		$19^+ \rightarrow 17^+$
802.8	19(1)		$21^+ \rightarrow 19^+$
863.0	12(0.7)		$22^+ \rightarrow 20^+$
885.5	15(0.9)		$23^+ \rightarrow 21^+$
948.6	8.2(6)		$24^+ \rightarrow 22^+$
968.5	10(0.7)		$25^+ \rightarrow 23^+$
1037.9	7.7(8)		$26^+ \rightarrow 24^+$
1056.1	9.5(8)		$27^+ \rightarrow 25^+$
1138	3.7(6)		$(28^+) \rightarrow 26^+$
1149	4.8(6)		$(29^+) \rightarrow 27^+$
1240	5.2(7)		$(31^+) \rightarrow (29^+)$
1246	2.6(6)		$(30^+) \rightarrow (28^+)$

[a]Relative intensities corrected for efficiency. The transition intensities were obtained from a combination of total projection and gated spectra.

[b]The tentative spin parity of the states are given in parentheses.

[c]Gated by a ''stretched'' dipole transition.

[d]Gated by a ''stretched'' quadrupole transition.

IV. DISCUSSION

A. Band properties and assignment

In order to assign the band to a specific configuration, we have drawn various physical quantities extracted from the experimental data for the lightest odd-odd Pr nuclei, such as the dynamical moments of inertia (Fig. 5), single-particle alignments (Fig. 6), the ratios of reduced transition probabilities $B(M1)/B(E2)$ (Fig. 7). They all indicate that the behavior of the band observed in ^{126}Pr is very similar to the

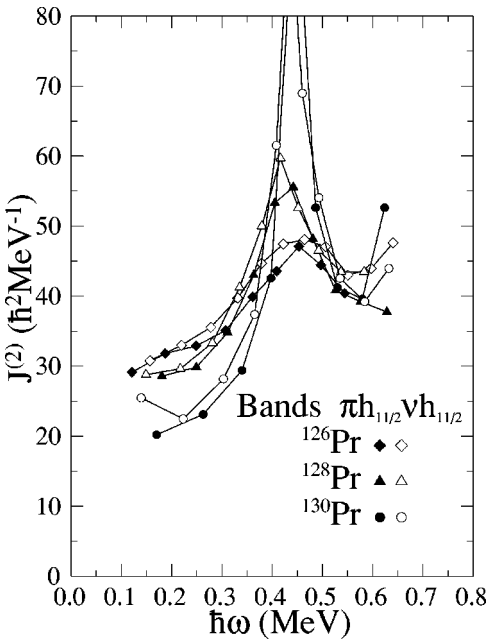

FIG. 5. Dynamical moments of inertia for the $\pi h_{11/2} \otimes \nu h_{11/2}$ bands of ^{126}Pr, ^{128}Pr, and ^{130}Pr. The two signatures $\alpha = 0$ and $\alpha = 1$ of each band are represented with open and closed symbols, respectively.

$\pi h_{11/2} \otimes \nu h_{11/2}$ bands of the heavier odd-odd Pr nuclei. We therefore assigned a $\pi h_{11/2} \otimes \nu h_{11/2}$ configuration to the band of ^{126}Pr. As one can see in Fig. 5, the dynamical moment of inertia of the ^{130}Pr, ^{128}Pr, and ^{126}Pr nuclei exhibit a perturbation at a rotational frequency $\hbar\omega \approx 0.45$ MeV, which is smoother in ^{126}Pr than in the heavier nuclei; furthermore, in the unperturbed region ($\hbar\omega \leqslant 0.4$ MeV) an increase of $J^{(2)}$ with decreasing neutron number is observed, which can be considered as an indication that the deformation increases when approaching the proton drip line. Note also that the $J^{(2)}$ values of ^{126}Pr are closer to ^{128}Pr than to ^{130}Pr, suggesting a closer resemblance between ^{126}Pr and ^{128}Pr. The dynamical moments of inertia are independent of spin, and therefore do not change when changing the spin assignment to the band. This is not the case for the single-particle alignments, which depend on both the core parameters and the spin assignments. The $J^{(2)}$ values in the unperturbed low-frequency region are $\sim 30\hbar^2$ MeV^{-1} for ^{126}Pr and ^{128}Pr, and $\sim 20\hbar^2$ MeV^{-1} for ^{130}Pr. These are the values used to extract the single-particle alignments drawn in Fig. 6. All three nuclei have similar aligned spins of around $7\hbar$ and present a crossing at a rotational frequency of around 0.45 MeV, which becomes smoother with decreasing neutron number. Note that the spins of ^{128}Pr have been changed by $\pm 1\hbar$ with respect to Ref. [7]. This spin change was imposed by the signature splitting of the $\pi h_{11/2} \otimes \nu h_{11/2}$ bands in the sequence of odd-odd Pr nuclei from ^{136}Pr to ^{126}Pr (see Fig. 8). The signature splitting of ^{126}Pr is in phase with those of the heavier Pr nuclei if one assigns either spin 8^+ or 6^+ to the lowest observed state. One would prefer the 8^+ assignment for two reasons: (i) a single-particle alignment similar to the other odd-odd Pr nuclei, which in the case of 6^+ assignment would be $2\hbar$ less for ^{126}Pr than for ^{128}Pr and ^{130}Pr (see Fig.

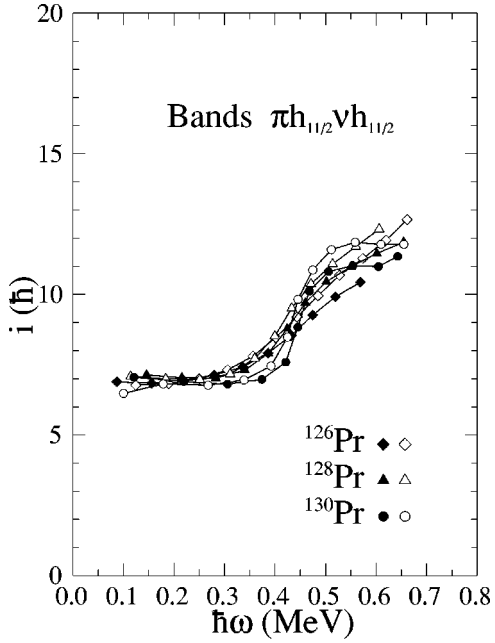

FIG. 6. Single particle alignments for the $\pi h_{11/2} \otimes \nu h_{11/2}$ bands of ^{126}Pr, ^{128}Pr, and ^{130}Pr. The parameters of the reference core are $J_0 = 30\hbar^2$ MeV^{-1}, $J_1 = 0\hbar^4$ MeV^{-3} for ^{126}Pr and ^{128}Pr, and $J_0 = 20\hbar^2$ MeV^{-1}, $J_1 = 20\hbar^4$ MeV^{-3} for ^{130}Pr. The band-head spins are 8^+ for ^{126}Pr, 9^+ for ^{128}Pr, and 7^+ for ^{130}Pr. The two signatures $\alpha = 0$ and $\alpha = 1$ of each band are represented with open and closed symbols, respectively.

6); (ii) the trend of the variation of the signature-inversion point is better satisfied for the 8^+ assignment than for the 6^+ one, since in the latter case the signature inversion for ^{128}Pr and ^{126}Pr occurs at spins which are equal or smaller by one unit, respectively, with respect to ^{130}Pr. The 8^+ spin assignment is also supported by the ratios of the reduced transition probabilities shown in Fig. 7, which show smaller values for ^{126}Pr with respect to ^{130}Pr. One can speculate that the smaller $B(M1)/B(E2)$ values of ^{126}Pr are due to the larger

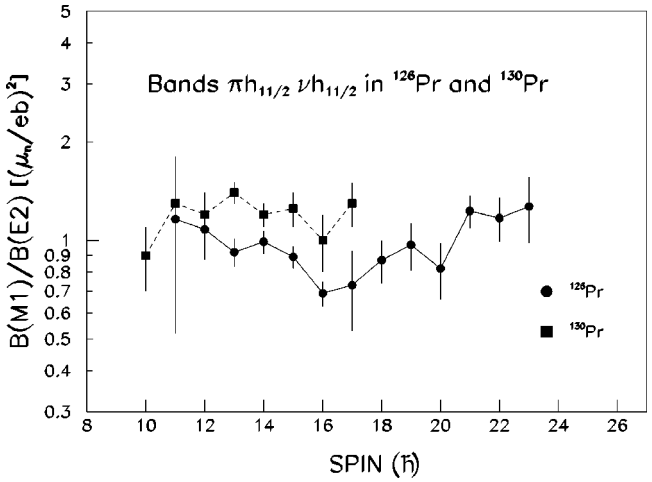

FIG. 7. Experimental branching ratios for the band observed in ^{126}Pr. For comparison, we also show the branching ratios of the $\pi h_{11/2} \otimes \nu h_{11/2}$ band of ^{130}Pr.

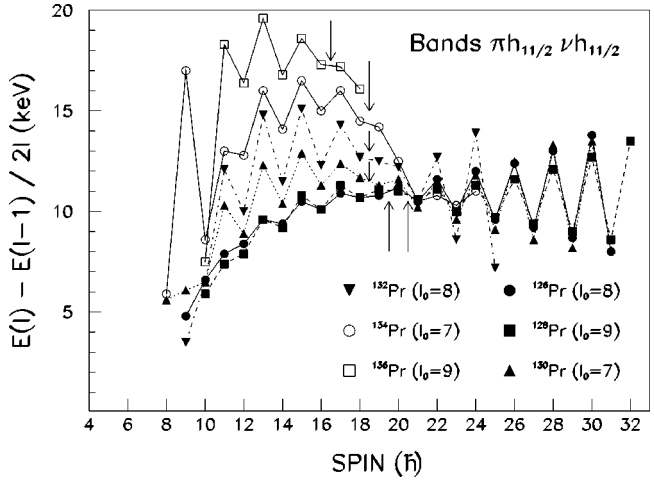

FIG. 8. Signature splitting of odd-odd Pr nuclei assuming spin 8^+ for the band head in ^{126}Pr. The arrows indicate the signature inversion points.

deformation, being the $B(M1)/B(E2)$ ratios proportional to $1/Q_0^2$. However, there is a problem with the 8^+ spin assignment: the systematics of the low-lying states in the odd-odd Pr nuclei shown in Fig. 9. For spin 6^+ one obtains a smooth decrease of the excitation energies when going towards lighter isotopes, which is due to the predicted increase in deformation when reducing the neutron number. For spin 8^+ one obtains instead a sudden decrease in excitation energy

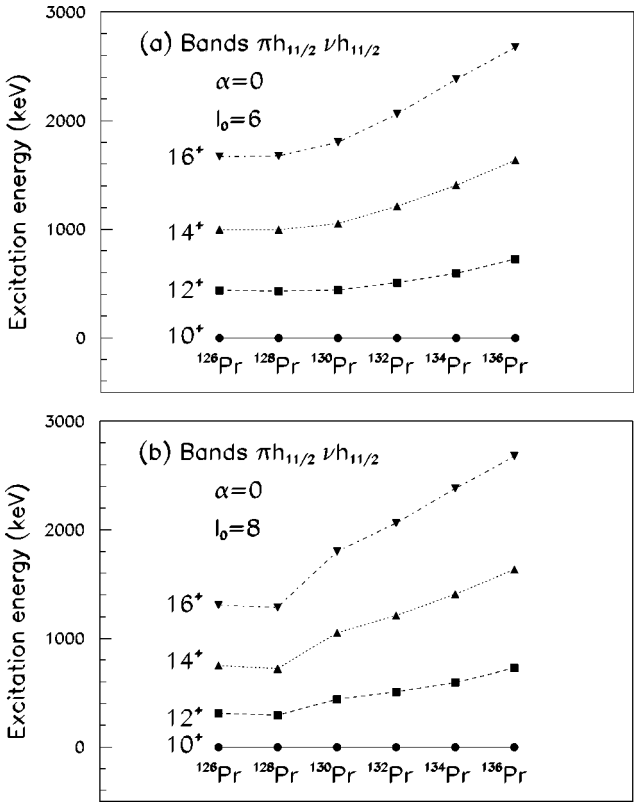

FIG. 9. Systematics of low-lying states in odd-odd Pr nuclei for spin 6^+ (left panel) and 8^+ (right panel). Note that the spins assigned to ^{128}Pr are as indicated in Fig. 8.

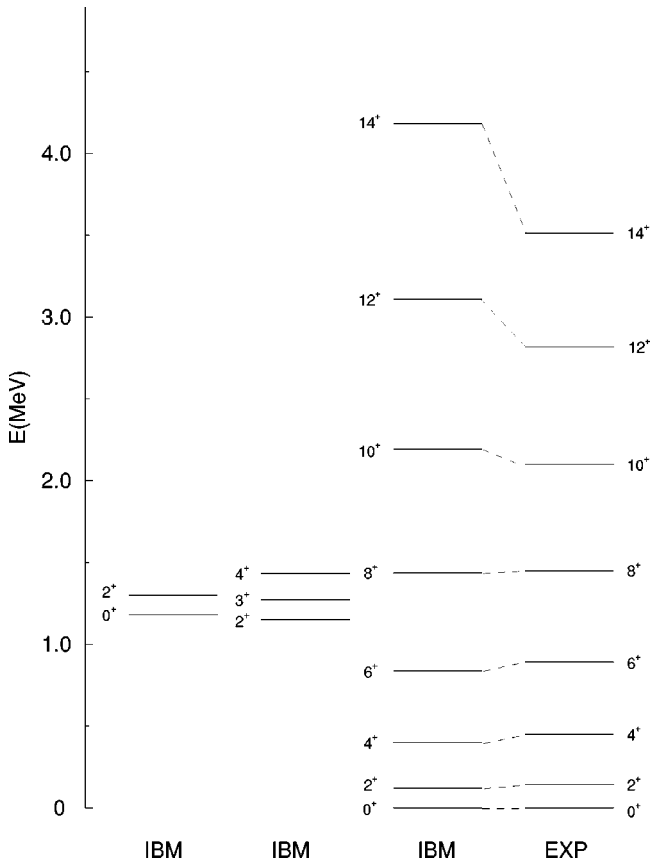

FIG. 10. Experimental yrast sequence of the core nucleus ^{124}Ce compared with the result of the IBM calculation.

between ^{130}Pr and ^{128}Pr, which remains nearly the same for ^{126}Pr. Is there any reason to have a sudden increase in deformation for ^{128}Pr, which would explain the decrease of the excitation energies for the 8^+ assignment? We believe that the answer to this question is not straightforward and an experimental measurement to establish the spin of the lowest observed state in ^{126}Pr is needed.

B. Interacting boson-fermion-fermion model analysis of the level structure of ^{126}Pr

The level structure of $^{126}_{59}\mathrm{Pr}_{67}$ is analyzed in the framework of the interacting boson fermion fermion model (IBFFM) [18]. A consistent procedure is employed which includes the analysis of the even-even and odd-even neighbors of ^{126}Pr. Positive-parity bands based on the proton $h_{11/2}$ and neutron $h_{11/2}$ and $f_{7/2}$ configurations are calculated. We included in the calculations only the $f_{7/2}$ configuration intruding from above the $N=82$ shell closure, being aware that at large deformation the $f_{7/2}$ and $h_{9/2}$ orbitals are mixed. The reason is that the energy of the $h_{11/2}$ states have nondiagonal contributions through the Y_2 operator which are large for the non-spin-flip matrix elements $\langle h_{11/2}|Y_2|f_{7/2}\rangle$ and small for the spin-flip matrix elements $\langle h_{11/2}|Y_2|h_{9/2}\rangle$. We have therefore ignored the contribution from the $h_{9/2}$ orbital.

The quasiparticle energies, occupation probabilities, and boson-fermion interaction strengths were determined by the interacting boson fermion model (IBFM) [19,20] analysis of negative parity states in $^{127}_{59}\mathrm{Pr}_{68}$ and $^{125}_{58}\mathrm{Ce}_{67}$. Likewise, the parameters which determine the structure of the positive parity states in ^{126}Pr based on the proton $d_{5/2}$, and $g_{7/2}$, and neutron $d_{3/2}$, $s_{1/2}$, $d_{5/2}$, and $g_{7/2}$ configurations, result from IBFM calculations of positive parity states in the odd-even and even-odd neighbors. In this way most model parameters are determined by the level structure of $^{127}_{59}\mathrm{Pr}_{68}$ and $^{125}_{58}\mathrm{Ce}_{67}$, and only the effective residual interaction between the odd proton and the odd neutron must be adjusted in order to reproduce the ^{126}Pr data. There could be, in addition, one or two parameters which, although in principle determined by the odd-A neighbors, have to be directly adjusted on the odd-odd nucleus. This happens, for instance, when available experimental data in the odd-A neighbors do not constrain the values of certain parameters. As the large number of bosons in the core nucleus $^{124}_{58}\mathrm{Ce}_{66}$ ($N=12$) implies a very large configuration space in the odd-odd nucleus, separate calculations have to be performed for the two sets of positive parity states based on the negative and on the positive parity single-proton and single-neutron orbitals. This is possible because there is very little mixing between the structure built on the negative parity orbitals ($\pi h_{11/2}$, $\nu h_{11/2}$, and $\nu f_{7/2}$) and the states based on positive parity proton and neutron orbitals. The experimental data, in fact, do not contain even the information about their relative position. For the states based on negative parity orbitals the calculation has been performed in the full boson space. On the other hand, due to the prohibitively large configuration space of states based on positive parity orbitals, these structures have been calculated in a truncated boson space. The Hamiltonian of the boson core had been prediagonalized, and the fermion orbitals have been coupled to the six lowest boson states of each angular momentum. We have verified that the resulting spectra and electromagnetic properties differ by no more than a few percent from those calculated with a full boson space. The interaction strength parameters used in the present analysis are defined in Ref. [21].

The core nucleus ^{124}Ce follows the systematic trend of the Ce isotopes. The heavier isotopes are γ soft [O(6)-like in the IBM terminology], and the lighter ones are considerably deformed, but they never reach the rigid rotor structure which corresponds to the SU(3) limit of the IBM. The transition between these two structures occurs for ^{126}Ce, and is reflected in the dynamics of bands in the neighboring odd-even and odd-odd nuclei. In contrast to the O(6)-like spectra observed in the odd-odd isotopes ^{130,132}Pr [22], the structure of ^{126}Pr reflects the transitional SU(3)-O(6) nature of the core nucleus ^{124}Ce. In the interacting boson model (IBM-1) [23,24] this type of transition is described by the Hamiltonian

$$H_{\mathrm{IBM}} = -\frac{\alpha}{10}QQ + \frac{\beta}{10}LL. \qquad (1)$$

The transition is determined by the value of the parameter χ in the quadrupole boson operator [23,24]. The limiting cases are $\chi=0$, which corresponds to the O(6) limit of the IBM-1, and $\chi=-\sqrt{7}/2$, which describes a prolate shape in the SU(3) dynamical symmetry limit. The spectrum of ^{124}Ce, displayed in Fig. 10, is calculated with $\alpha=0.19$ MeV, β

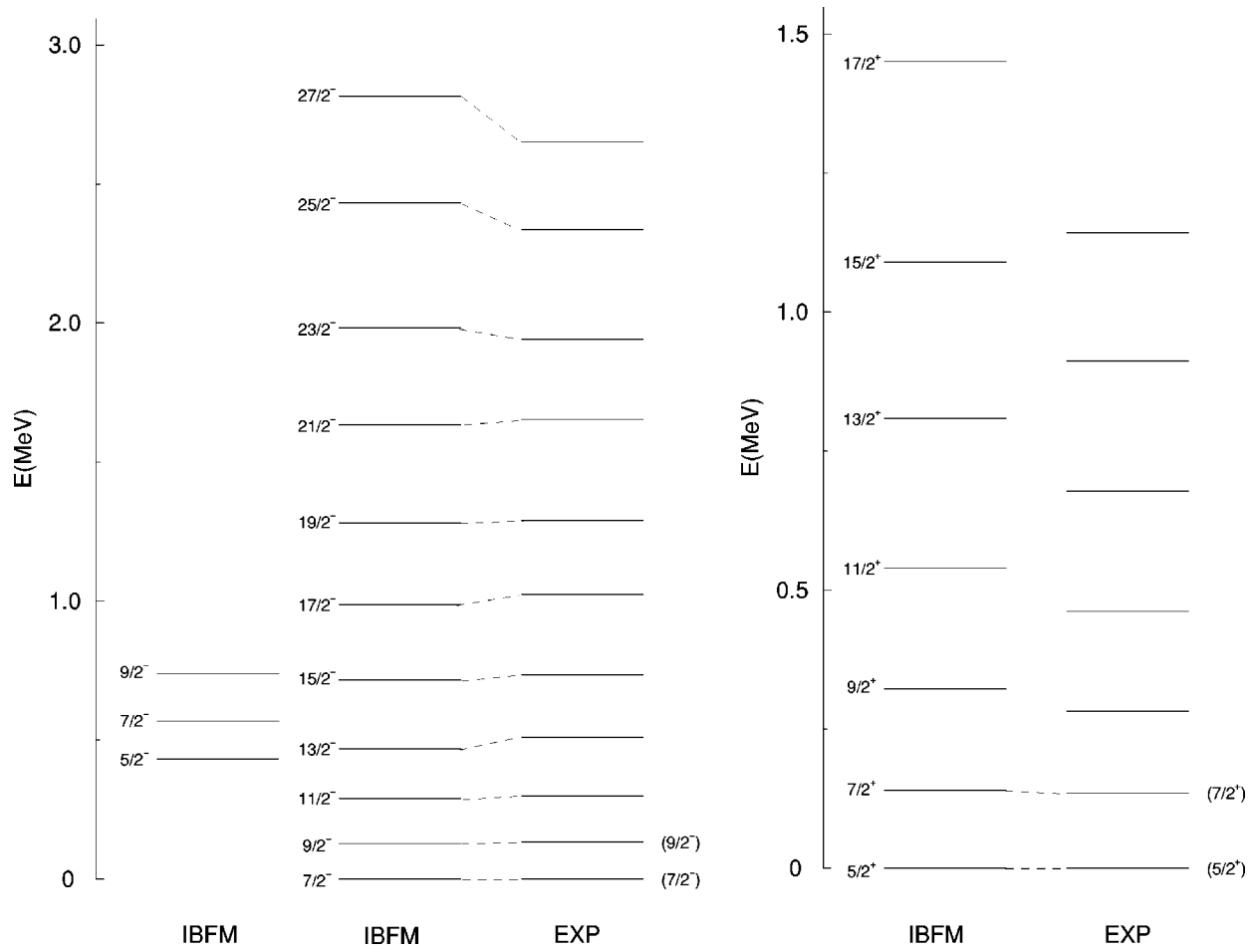

FIG. 11. The negative parity (a) and positive parity (b) yrast states in the odd-N nucleus ^{125}Ce compared with the spectra calculated with the IBF model.

$=0.13$ MeV, and $\chi=-1.0$. The calculated spectrum is in good agreement with the experimental data up to angular momentum $I=10$. The yrast states above $I=10$ should be based on two-quasiparticle configurations, either two-proton states or two-neutron states coupled to the boson core. These states are not included in the model space of the present analysis. The same values of the parameters of the boson Hamiltonian are used in the IBFM calculations of $^{125}_{59}\mathrm{Pr}_{66}$ and $^{125}_{58}\mathrm{Ce}_{67}$, and in the IBFFM analysis of ^{126}Pr. In addition, the value $\chi=-1.0$ is also used in the boson operator of the fermion-boson quadrupole interaction, as well as in the $E2$ boson operator. The boson vibrational charge (defined in Ref. [25]) $e^{\mathrm{vib}}=0.95$ is obtained from the value that has been used in the calculation of ^{130,132}Pr in Ref. [22], by scaling with the square root of the boson number. The standard value $g_R=Z/A$ is used for the gyromagnetic ratio g_R.

In the IBFM analysis of the odd-N nucleus $^{125}_{58}\mathrm{Ce}_{67}$ the following neutron quasiparticle energies ε and occupation probabilities v^2 have been used: $\varepsilon(\nu h_{11/2})=1.32$ MeV, $\varepsilon(\nu s_{1/2})=1.49$ MeV, $\varepsilon(\nu d_{5/2})=1.52$ MeV, $\varepsilon(\nu g_{7/2})=1.63$ MeV, $\varepsilon(\nu d_{3/2})=1.64$ MeV, $v^2(\nu h_{11/2})=0.40$, $v^2(\nu s_{1/2})=0.25$, $v^2(\nu d_{5/2})=0.76$, $v^2(\nu g_{7/2})=0.80$, $v^2(\nu d_{3/2})=0.19$. These values result from a BCS calculation with the particle energies taken from Ref. [26] for $N=69$, and $G=23/A$ MeV for the strength of the pairing interaction. The same set of quasiparticle energies was also used in the IBFFM calculation of ^{124}Cs [27]. In addition, in the present calculation we have included the $\nu f_{7/2}$ orbital from the shell above, with $\varepsilon(\nu f_{7/2})=5.32$ MeV, $v^2(\nu f_{7/2})=0.01$. The strength parameters of the boson-fermion interaction are (all values in MeV): $A_0^\nu=0.12, \Gamma_0^\nu=0.4, \Lambda_0^\nu=4.0$ for positive parity states, and $A_0^\nu=0.08, \Gamma_0^\nu=0.4, \Lambda_0^\nu=1.3$ for states of negative parity. For negative parity, the strength parameters are similar to those of ^{131}Ce [22], and very close to the values used for ^{123}Xe and ^{124}Cs [27]. The calculated spectrum of negative parity states is compared with experimental data in Fig. 11(a). Although the doublet structure of the band based on $7/2_1^-$ is slightly more pronounced in the experimental spectrum, an excellent agreement is found up to angular momentum $I=27/2^-$. The available data set on electromagnetic properties in ^{125}Ce [28] is very limited. We have used the neutron gyromagnetic ratios $g_l^\nu=0, g_s^\nu=0.5 g_s^{\nu,\mathrm{free}}=-1.913$, and the standard effective neutron charge $e^\nu=0.5$ from Ref. [22]. The results of the present calculation for positive parity states in ^{125}Ce [Fig. 11(b)] support the $[402]5/2^+$ assignment for the ground state band [28]. The dominant spherical configuration is $\nu g_{7/2}$, with a significant

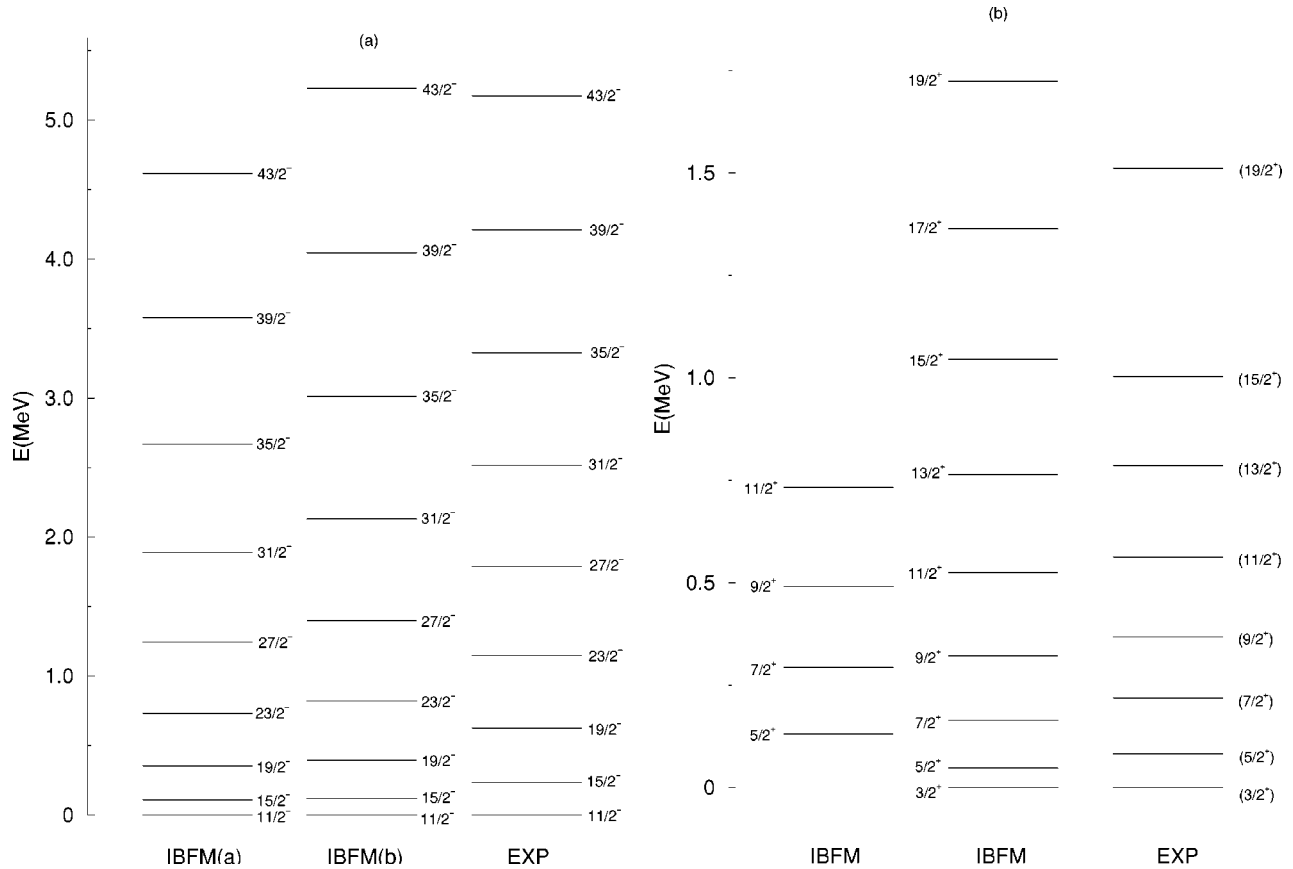

FIG. 12. The negative parity (a) and positive parity (b) yrast states in the odd-Z nucleus ^{125}Pr are compared with the experimental states of ^{127}Pr. For description see the text.

admixture of $\nu d_{5/2}$ components. The contribution of $\nu d_{5/2}$ gets larger with increasing angular momentum in the band. Unfortunately, the very limited experimental data on positive parity states in ^{125}Ce do not allow a precise determination of the boson-fermion interaction strengths. The values of the boson-proton interaction strengths should be, in principle, determined by the spectrum of the odd-Z nucleus $^{125}_{59}\mathrm{Pr}_{66}$. However, no experimental data are available at present and we have, therefore, based our analysis on the heavier isotopes ^{127,129}Pr. In the calculation of negative parity states the occupation probability of the proton orbital is $v^2(\pi h_{11/2}) = 0.06$ [22], and the boson-fermion interaction strengths (all values in MeV): $\Gamma_0^\pi = 0.25$ and $\Lambda_0^\pi = 3.0$. These values have also been employed in the calculation of ^{126}Pr. The strength parameter of the monopole interaction is, however, not uniquely determined from the spectra of ^{127,129}Pr. We have analyzed two values $A_0^\pi = 0.14$ MeV (suitable for ^{127}Pr) and $A_0^\pi = 0.03$ MeV (the last value was also used in the calculation of ^{129}Pr). In Fig. 12(a) the corresponding spectra are denoted IBFM(a) and IBFM(b), respectively. The calculated bands are compared with the experimental band in ^{127}Pr based on $11/2_1^-$. The calculated spectra reflects a change of deformation that is expected to occur close to the proton drip line, being related to the transition in the core even-even nuclei. In the following calculations we have employed $A_0^\pi = 0.14$ MeV, a value which is suitable for the expected more deformed ^{125}Pr. The values of the proton gyromagnetic factors $g_l^\pi = 1.0$, $g_s^\pi = 0.5$, $g_s^{\pi,\mathrm{free}} = 2.793$, and the standard proton charge $e^\pi = 1.0$, are the same as those used in Ref. [22].

The experimental data on proton positive parity states in ^{127}Pr are not sufficient to establish the absolute excitation energies of the observed band with respect to the negative parity band [6]. In our calculation of ^{126}Pr we have, therefore, made a reasonable assumption that the quasiparticle energy of $\pi h_{11/2}$ is ≈ 0.6 MeV above the $\pi d_{5/2}$ quasiparticle energy. With the occupation probabilities from Ref. [22]: $v^2(\pi d_{5/2}) = 0.40, v^2(\pi g_{7/2}) = 0.71$, and by slightly increasing the difference between quasiparticle energies $\varepsilon(\pi g_{7/2}) - \varepsilon(\pi d_{5/2})$ from 0.18 to 0.4 MeV, a very good agreement with the experimental data of ^{127}Pr is obtained [Fig. 12(b)]. The ground state band based on the $\pi g_{7/2}$ and $\pi d_{5/2}$ configurations confirms the $[411]3/2^+$ assignment of Ref. [6] and is in agreement with the systematics of odd-A Pr isotopes.

The deduced boson-fermion interaction strengths for unique parity orbitals can be compared to the values in typical deformed nuclei in other parts of the chart of nuclides. Instead of comparing A_0, Γ_0, and Λ_0, it is better to compare the total interaction strengths A_j, Γ_{jj}, and Λ_{jj}^j [29]. The total monopole strength (-0.1) is equal in ^{129}Pr, ^{151}Pm [29], and ^{181}Re [30]. The values of the total dynamical and exchange boson-proton interaction strengths are -0.53 and -1.02 in the present calculation, -1.25 and -5.48 in ^{151}Pm [29], 0.43 (positive sign is due to the holelike nature of the

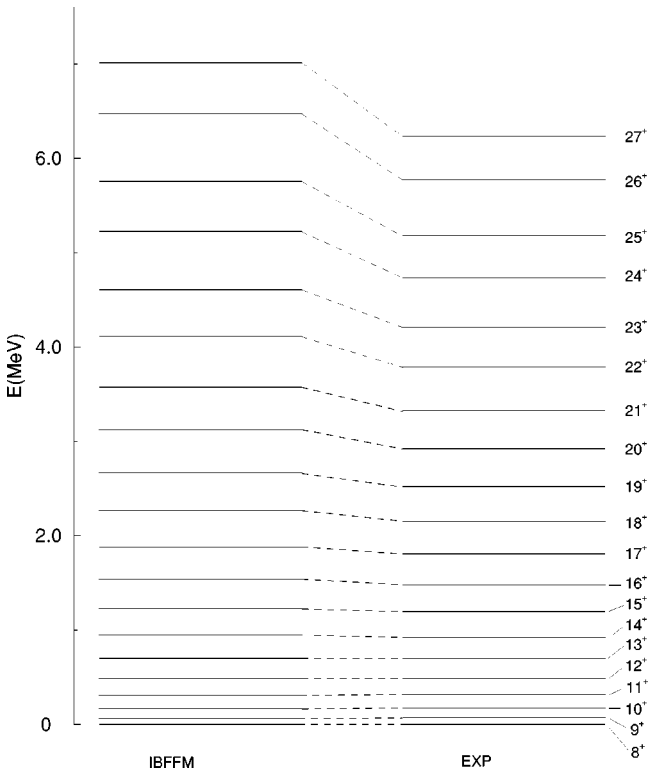

FIG. 13. The yrast sequence of high angular momentum positive parity states based on the $\pi h_{11/2} \otimes \nu h_{11/2}$ configuration is compared with its experimental counterpart in ^{126}Pr. The assignment for the band head, i.e., the lowest observed state is 8^+.

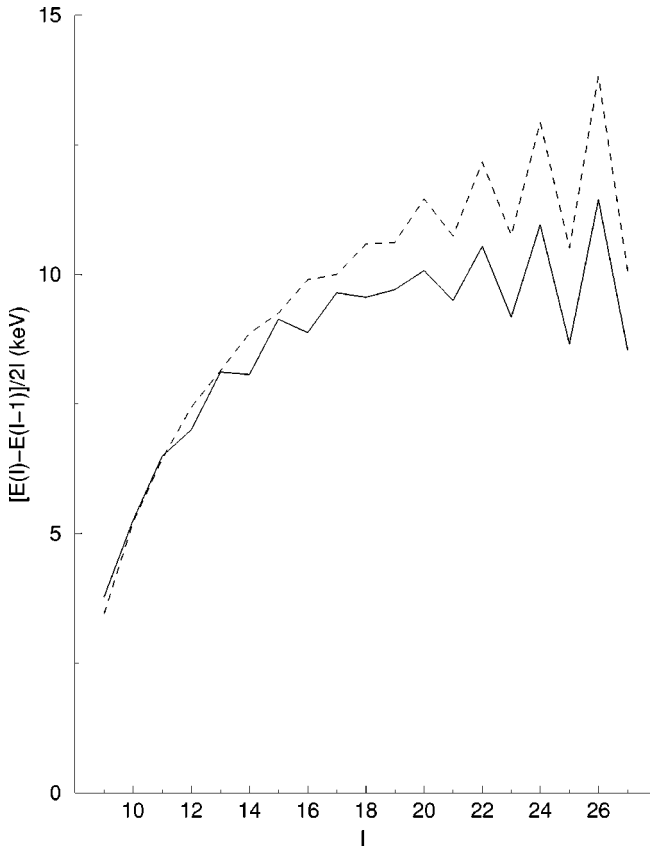

FIG. 14. The IBFFM (dashed line) and the experimental (solid line) $[E(I)-E(I-1)]/2I$ vs I plots for the $\pi h_{11/2} \otimes \nu h_{11/2}$ yrast band in ^{126}Pr. The state 8^+ is assigned to the band head.

$h_{11/2}$ proton), and -1.99 in ^{181}Re [30]. For boson-neutron interaction strengths the respective values are -0.19 and -1.88 in the present calculation and -0.32 and -4.33 in ^{181}Os [30]. The absolute values differ due to different moments of inertia of the respective cores but a systematic behavior is preserved in all cases, the total strength of the exchange interaction is several times bigger than the total strength of the dynamical interaction.

Very few parameters remain to be adjusted in the final calculation of ^{126}Pr. For the effective residual odd-proton–odd-neutron interaction the spin-spin force has been used with the strength $V_{\sigma\sigma}=0.5$ MeV. In order to reproduce the change of signature pattern observed in the yrast sequence of ^{126}Pr, an additional η term has been included in the boson operator of the dynamical boson-fermion interaction. This additional term and its polarization effects have been discussed in Ref. [31] for the spectra of ^{130,132}Pr. In the present calculation the parameter of the η term is 0.02 MeV.

In Fig. 13 the calculated high-spin band based on the $\pi h_{11/2} \otimes \nu h_{11/2}$ configuration is compared with the experimental sequence of yrast states in ^{126}Pr. The moment of inertia and the observed staggering above spin $I=18^+$ (Fig. 14) is well described by the model calculation. The results shown in Figs. 13 and 14 are consistent with the 8^+ assignment for the lowest observed level. In Table II we have compared the calculated and experimental transition intensities for this structure. An excellent agreement is found between the experimental values and the theoretical predictions for the electromagnetic transition properties of the yrast sequence. We notice that the calculation predicts a 7^+ state based on the $\pi h_{11/2} \otimes \nu h_{11/2}$ configuration 12 keV below the 8^+ band-head state. This energy difference is too small to be observed in experiment. On the other hand, the relative positions of the 7^+ and the 8^+ states can be influenced by terms in the proton-neutron interaction that are not included in the present calculation.

The calculated spectrum of states based on positive parity proton and neutron configurations is shown in Fig. 15. As we have emphasized above, the limited experimental information on the odd-A neighbors does not allow a precise determination of relative excitation energies with respect to the yrast $\pi h_{11/2} \otimes \nu h_{11/2}$ band. The results of the present calculation indicate that the observed $(\pi h_{11/2} \otimes \nu h_{11/2})$ 8^+ is not the ground state. We suggest an excitation energy of ≈ 400 keV, or lower, for this state. A higher excitation energy would imply a very weak transition to the 6_1^+ state calculated at ≈ 400 keV (Fig. 15), which has not been observed in experiment. We conclude, therefore, that 8_1^+ is an isomeric state. Consequently, the ground state must be based on positive parity proton and neutron orbitals. The present analysis, as well as the Gallagher-Moszkowsky rule, strongly favors the state 1^+. The sequence displayed in Fig. 17 (1^+ ground state, followed by a doublet 0^+, 2^+) is very stable for various choices of the residual proton-neutron interaction. Nevertheless, there is a possibility that the ground state

TABLE II. Electromagnetic transition properties of yrast states in ^{126}Pr. The first column identifies the transition by its initial and final angular momentum and parity assignments. In the second and third columns the theoretical $B(E2)$ and $B(M1)$ transition probabilities are displayed, respectively. The experimental and IBFFM γ intensities are compared in the last two columns.

	IBFFM		I_γ	
Transition	$B(E2)(e^2\,b^2)$	$B(M1)(\mu_N^2)$	exp.	IBFFM
$9_1^+ \to 8_1^+$	0.4314	0.5942	100	100
$10_1^+ \to 9_1^+$	0.3874	0.5006	100	100
$10_1^+ \to 8_1^+$	0.2584			5
$11_1^+ \to 10_1^+$	0.3367	0.4538	100	100
$11_1^+ \to 9_1^+$	0.3069		21	15
$12_1^+ \to 11_1^+$	0.2889	0.4214	100	100
$12_1^+ \to 10_1^+$	0.3466		28	35
$13_1^+ \to 12_1^+$	0.2458	0.4088	100	100
$13_1^+ \to 11_1^+$	0.3785		65	52
$14_1^+ \to 13_1^+$	0.2095	0.3896	100	100
$14_1^+ \to 12_1^+$	0.4021		96	97
$15_1^+ \to 14_1^+$	0.1778	0.3931	84	91
$15_1^+ \to 13_1^+$	0.4207		100	100
$16_1^+ \to 15_1^+$	0.1519	0.3714	42	54
$16_1^+ \to 14_1^+$	0.4316		100	100
$17_1^+ \to 16_1^+$	0.1291	0.3881	43	53
$17_1^+ \to 15_1^+$	0.4409		100	100
$18_1^+ \to 17_1^+$	0.1107	0.3540	37	35
$18_1^+ \to 16_1^+$	0.4413		100	100
$19_1^+ \to 18_1^+$	0.0940	0.3882	38	35
$19_1^+ \to 17_1^+$	0.4447		100	100
$20_1^+ \to 19_1^+$	0.0806	0.3309	25	26
$20_1^+ \to 18_1^+$	0.4457		100	100
$21_1^+ \to 20_1^+$	0.0683	0.3901	34	25
$21_1^+ \to 19_1^+$	0.4360		100	100
$22_1^+ \to 21_1^+$	0.0581	0.2979	35	22
$22_1^+ \to 20_1^+$	0.4171		100	100
$23_1^+ \to 22_1^+$	0.0490	0.3927	25	19
$23_1^+ \to 21_1^+$	0.4176		100	100
$24_1^+ \to 23_1^+$	0.0408	0.2526		18
$24_1^+ \to 22_1^+$	0.3872		100	100
$25_1^+ \to 24_1^+$	0.0344	0.3929		15
$25_1^+ \to 23_1^+$	0.3909		100	100
$26_1^+ \to 25_1^+$	0.0273	0.1972		15
$26_1^+ \to 24_1^+$	0.3471		100	100
$27_1^+ \to 26_1^+$	0.0235	0.3895		12
$27_1^+ \to 25_1^+$	0.3562		100	100
$28_1^+ \to 27_1^+$	0.0170	0.1393		11
$28_1^+ \to 26_1^+$	0.2970		100	100
$29_1^+ \to 28_1^+$	0.0158	0.3849		9
$29_1^+ \to 27_1^+$	0.3108		100	100
$30_1^+ \to 29_1^+$	0.0097	0.0910		9
$30_1^+ \to 28_1^+$	0.2377		100	100
$31_1^+ \to 30_1^+$	0.0107	0.3899		8
$31_1^+ \to 29_1^+$	0.2506		100	100

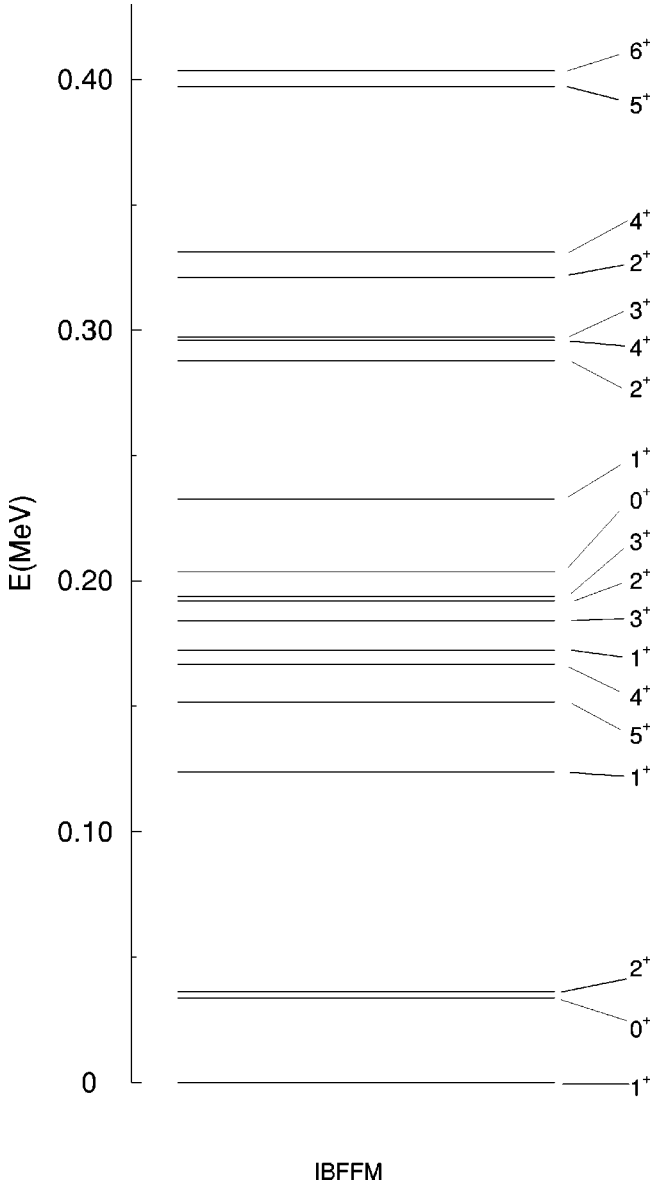

FIG. 15. The IBFFM prediction for low angular momentum states in ^{126}Pr. These states are based on positive parity proton and neutron configurations.

is 0^+, or even 2^+.

The IBFFM analysis predicts the existence of another isomer in ^{126}Pr: 5^+ at ≈ 150 keV excitation energy. Its isomeric character depends strongly on the choice of the proton-neutron interaction. In the present calculation, 5_1^+ is below 4_1^+ (Fig. 15), and therefore it is an isomer with a possible γ decay to 2_1^+. This transition is slow enough to allow for a β decay that has been reported in Ref. [10].

We have also analyzed the possibility that the band-head of the high-spin band $\pi h_{11/2} \otimes \nu h_{11/2}$ is 6^+. We have used $A_0^\pi = 0.03$ MeV (taken from the calculation of ^{129}Pr) for the strength of the monopole interaction, and slightly changed the boson-neutron interaction to $\Gamma_0^\nu = 0.43$ MeV and $\Lambda_0^\nu = 1.55$ MeV. In the dynamical boson-fermion interaction $\eta = 0$ and, instead of the spin-spin force, a residual interaction of tensor type has been used with the strength parameter

$V_T = -0.03$ MeV. Comparing the behavior of the moment of inertia and signature splitting in the results of our calculations that gave band heads 8^+ and 6^+, respectively, we notice that the agreement with experimental data is somewhat better for the 8^+ band head. Our calculations, however, cannot exclude the 6^+ assignment for the lowest observed state of the $\pi h_{11/2} \otimes \nu h_{11/2}$ is 6^+ structure.

V. CONCLUSIONS

We observed for the first time excited states in the near drip-line nucleus ^{126}Pr, which form a regular rotational band up to quite high spin. The observed level structures have been discussed in the framework of the interacting boson-fermion-fermion model.

[1] C. N. Davids *et al.*, Phys. Rev. Lett. **80**, 1849 (1998).

[2] P. Möller, J.R. Nix, W.D. Myers, and W.J. Swiatecki, At. Data Nucl. Data Tables **59**, 185 (1995).

[3] D. Vretenar, G.A. Lalazissis, and P. Ring, Phys. Rev. Lett. **82**, 4595 (1999).

[4] E. Maglione, L.S. Ferreira, and R.J. Liotta, Phys. Rev. Lett. **81**, 538 (1998).

[5] S. Hofmann (unpublished).

[6] S.M. Mullins, A. Galindo-Uribarri, C.E. Svensson, R.A.E. Austin, G.C. Ball, M. Cromaz, V.P. Janzen, D.C. Radford, I. Ragnarsson, J.C. Waddington, and D. Ward, Phys. Rev. C **58**, R2626 (1998).

[7] B.H. Smith, L.L. Riedinger, H.Q. Jin, W. Reviol, W. Satula, A. Galindo-Uribarri, D.G. Sarantites, J.N. Wilson, D. LaFosse, and S.M. Mullins, Phys. Lett. B **443**, 89 (1998).

[8] C. Rossi Alvarez, Nuc. Phys. News **3**, 10 (1993).

[9] J.M. Nitschke, M.D. Cable, and W.-D. Zeitz, Z. Phys. A **312**, 265 (1983).

[10] D. Barnéoud, J. Blachot, J. Genevey, A. Gizon, R. Béraud, R. Duffait, A. Emsallem, M. Meyer, N. Redon, and D. Rolando-Eugio, Z. Phys. A **330**, 341 (1988).

[11] A. Osa, M. Asai, M. Koizumi, T. Sekine, S. Ichikawa, Y. Kojima, H. Yamamoyo, and K. Kawade, Nucl. Phys. **A588**, 185c (1995).

[12] C.M. Petrache, G. Lo Bianco, G. Falconi, A. Saltarelli, M. Nespolo, D. Bazzacco, F. Fanzago, T. Kröll, S. Lenzi, S. Lunardi, E. Maglione, R. Menegazzo, P. Pavan, S. Quintana, G. Rigadello, C. Rossi Alvarez, P. Spolaore, G. de Angelis, M. De Poli, N. Marginean, T. Martinez, M. Axiotis, D.R. Napoli, and N. Blasi (unpublished).

[13] C.M. Petrache, G. Lo Bianco, A. Saltarelli, M. Nespolo, D. Bazzacco, T. Kröll, S. Lunardi, E. Maglione, R. Menegazzo, S. Quintana, P. Spolaore, M. Axiotis, G. de Angelis, N. Marginean, T. Martinez, D.R. Napoli, and N. Blasi, *Proceedings of the International Workshop Symmetries and Spin PRAHA-SPIN-2000*, Praga, Czech Republic, 2000 [Czech J. Phys., Sect. A **51**, 261 (2001)].

[14] D.J. Hartley, A. Galindo-Uribarri, C. Baktash, M.P. Carpenter, M. Danchev, M. Devlin, C.J. Gross, R.V.F. Janssens, M. Lipoglavsek, E. Padilla, S.D. Paul, D.C. Radford, W. Reviol, L.L. Riedinger, D.G. Sarantites, D. Seweryniak, C.-H. Yu, and O. Zeidan, Phys. Rev. C **63**, 041301(R) (2001).

[15] E. Farnea, G. de Angelis, D. De Acuna, A. Gadea, D.R. Napoli, P. Spolaore, A. Buscemi, R. Zanon, R. Isocrate, D. Bazzacco, C. Rossi Alvarez, P. Pavan, A.M. Bizzetti-Sona, and P.G. Bizzetti, Nucl. Instrum. Methods Phys. Res. A **400**, 87 (1997).

[16] P. Spolaore, D. Ackermann, P. Bednarczyk, G. De Angelis, D. Napoli, C. Rossi Alvarez, D. Bazzacco, R. Burch, L. Müller, G.F. Segato, and F. Scarlassara, Nucl. Instrum. Methods Phys. Res. A **359**, 500 (1995).

[17] C.M. Petrache, D. Bazzacco, S. Lunardi, C. Rossi Alvarez, G. de Angelis, M. De Poli, D. Bucurescu, C.A. Ur, P.B. Semmes, and R. Wyss, Nucl. Phys. **A597**, 106 (1996).

[18] V. Paar, in *Capture Gamma-ray Spectroscopy and Related Topics*, edited by S. Raman, AIP Conf. Proc. No. 125 (AIP, New York, 1985), p. 70; S. Brant, V. Paar, and D. Vretenar, Z. Phys. A **319**, 355 (1984); V. Paar, D.K. Sunko, and D. Vretenar, *ibid.* **291**, 327 (1987); S. Brant and V. Paar, *ibid.* **329**, 151 (1988).

[19] F. Iachello and O. Scholten, Phys. Rev. Lett. **43**, 679 (1979).

[20] F. Iachello and P. Van Isacker, *The Interacting Boson Fermion Model* (Cambridge University Press, Cambridge, 1991).

[21] J. Timár, T.X. Quang, T. Fényes, Zs. Dombrádi, A. Krasznahorkay, J. Kumpulainen, R. Julin, S. Brant, V. Paar, and Lj. Šimičić, Nucl. Phys. **A573**, 61 (1994).

[22] C.M. Petrache, S. Brant, D. Bazzacco, G. Falconi, E. Farnea, S. Lunardi, V. Paar, Zs. Podolyák, R. Ventureli, and D. Vretenar, Nucl. Phys. **A635**, 361 (1998).

[23] F. Iachello and A. Arima, *The Interacting Boson Model* (Cambridge University Press, Cambridge, 1987).

[24] A. Arima and F. Iachello, Phys. Rev. Lett. **35**, 157 (1975); Ann. Phys. (N.Y.) **99**, 233 (1976); **111**, 201 (1978); **123**, 468 (1979).

[25] Y. Tokunaga, H. Seyfarth, O.W.B. Schult, S. Brant, V. Paar, D. Vretenar, H.G. Börner, G. Barreau, H. Faust, Ch. Hofmeyr, K. Schreckenbach, and R.A. Meyer, Nucl. Phys. **A430**, 269 (1984).

[26] Gh. Cata-Danil, D. Bucurescu, A. Gizon, and J. Gizon, J. Phys. G **20**, 1051 (1994).

[27] A. Gizon, J. Timár, J. Gizon, B. Weiss, D. Barnéoud, C. Foin, J. Genevey, F. Hannachi, C.F. Liang, A. Lopez-Martens, P. Paris, B.M. Nyakó, L. Zolnai, J.C. Merdinger, S. Brant, and V. Paar, Nucl. Phys. A (to be published).

[28] E.S. Paul, A.J. Boston, A. Galindo-Uribarri, T.N. Ginter, C.J. Gross, A.N. James, P.J. Nolan, R.D. Page, S.D. Paul, A. Piechaczek, D.C. Radford, W. Reviol, L.L. Riedinger, H.C. Scraggs, W. Weintraub, and C.-H. Yu, Phys. Rev. C **58**, 801 (1998).

[29] O. Scholten and T. Ozzello, Nucl. Phys. **A424**, 221 (1984).

[30] W.-T. Chou, Wm.C. McHarris, and O. Scholten, Phys. Rev. C **37**, 2834 (1988).

[31] C.M. Petrache, R. Venturelli, D. Vretenar, D. Bazzacco, G. Bonsignori, S. Brant, S. Lunardi, N.H. Medina, M.A. Rizzutto, C. Rossi Alvarez, G. de Angelis, M. De Poli, and D.R. Napoli, Nucl. Phys. **A617**, 228 (1997).